Sensitivity analysis for the detection NO_2 plumes from seagoing ships using TROPOMI data

Solomiia Kurchaba[a], Artur Sokolovsky[b], Jasper van Vliet[c], Fons J. Verbeek[a], Cor J. Veenman[a,d]

[a]*Leiden Institute of Advanced Computer Science (LIACS), Leiden University, Niels Bohrweg 1, Leiden, 2333 CA, The Netherlands*
[b]*School of Computing, Newcastle University, 1 Science Square, Newcastle-upon-Tyne, NE45TG, UK*
[c]*Human Environment and Transport Inspectorate (ILT), Graadt van Roggenweg 500, Utrecht, 3531 AH, The Netherlands*
[d]*Data Science Department, TNO, Anna van Buerenplein 1, The Hague, 2595 DA, The Netherlands*

Abstract

The marine shipping industry is among the strong emitters of nitrogen oxides (NO_x) – a substance harmful to ecology and human health. Monitoring of emissions from shipping is a significant societal task. Currently, the only technical possibility to observe NO_2 emission from seagoing ships on a global scale is using TROPOMI data. A range of studies reported that NO_2 plumes from some individual ships can be visually distinguished on selected TROPOMI images. However, all these studies applied subjectively established pre-determined thresholds to the minimum speed and length of the ship – variables that to a large extent define the emission potential of a ship. In this study, we investigate the sensitivity limits for ship plume detection as a function of their speed and length using TROPOMI data. For this, we train a classification model to distinguish TROPOMI image patches with a ship, from the image patches, where there were no ships. This way, we exploit ground truth ship location data to potentially exceed human visual distinguishability. To test for regional differences, we study four regions: the Mediterranean Sea, Biscay Bay, Arabian Sea, and Bengal Bay. For the Mediterranean and the Arabian Sea, we estimate the sensitivity limit to lie around a minimum speed of 10 knots and a minimum length of 150 meters. For the Biscay Bay – around 8 knots and 100 meters. We further show that when focusing the analysis on the biggest emitters (junctions of several ships in the area), the detectability can be improved up to above 0.8 ROC-AUC. Finally, we show that increasing the size of the dataset, beyond the dataset used in this study, yields further improvements in the detectability of smaller/slower ships. The rate of improvement in both experiments is dependent on the region studied. This paper is the first comprehensive study on the real-world sensitivity of the TROPOMI instrument to distinguish the NO_2 emission produced by seagoing ships.

Keywords: TROPOMI, sensitivity limits, machine learning, emissions, seagoing ships, NO2

1. Introduction

International shipping is one of the biggest emitters of nitrogen oxides (NO_x). The increased abundance of these gases in the atmosphere causes severe damage to human health and ecology (Corbett et al., 2007). To mitigate the negative effects caused by the shipping industry, International Maritime Organization (IMO) introduced incremental restrictions on emission levels that can be produced by individual seagoing ships (IMO, 1997, 2020). However, monitoring of ship emissions on a large scale remains a challenging task, as current compliance methods have serious limitations. For instance, port state authorities conduct checks on engine room logs, and bunker delivery notes, as well as take fuel samples, but these practices are applied to only a limited number of ships. Other applied methods are on-board measurements at exhaust pipes (Agrawal et al., 2008), land- or ship-based downwind measurements using sniffer techniques (Lack et al., 2009; Pirjola et al., 2014), and the DOAS (differential optical absorption spectroscopy) approach (McLaren et al., 2012; Schreier et al., 2015). Alternatively, ship plume measurements are performed from airborne platforms like helicopters, small aircraft, and drones (Van Roy and Scheldeman, 2016). Mobile platforms often measure pollutant ratios during plume transects (Beecken et al., 2014) or use the DOAS technique for remote optical sensing (Berg et al., 2012). Nevertheless, these methods require proximity to the studied ships, are applied sporadically, and are too costly for monitoring a global shipping fleet. As a result, there is no effective method for comprehensive and cost-efficient large-scale ship emission monitoring.

Several studies reported that with the TROPOspheric Monitoring Instrument on board the Copernicus Sentinel 5 Precursor (TROPOMI/S5P) satellite (Veefkind et al., 2012), some plumes from individual ships can be visually distinguished (Georgoulias et al., 2020; Kurchaba et al., 2021, 2022, 2023). However, in all those studies, the authors applied a pre-determined threshold on the minimum speed or length of the ship – the variables that are determinants of the level of ship emission potential. By setting such thresholds, ships whose NO_2 plumes are unlikely to be detected are left out of the dataset. For instance, in (Georgoulias et al., 2020) the authors studied several days of

TROPOMI measurements in the Mediterranean Sea, while visually analyzing ship plumes from ships longer than 200 meters (m). In (Kurchaba et al., 2021), a threshold-based ship plume segmentation approach was applied on several days of measurement from the Arabian and Mediterranean Seas. The studied ships were longer than 150 m and sailed faster than 12 knots (kt). In (Kurchaba et al., 2022), a machine-learning-based ship plume segmentation model was applied to eight months of TROPOMI measurements. While the approach allows quantification of emission intensity, only ships with a speed above 14 kt were analyzed. In (Kurchaba et al., 2023), we presented an approach for the automated identification of anomalous emitters. Only ships with a length over 150 m and a speed exceeding 12 kt were taken into account. In summary, to this moment, there is no study that investigates the global/regional sensitivity of the TROPOMI instrument with respect to the NO_2 emission produced by individual seagoing ships related to their speed and length.

In this study, we investigate the sensitivity limits of a detection system for NO_2 plumes from seagoing ships using TROPOMI data. To tackle the problem, we prepare image patches – small, regular-sized sections of the TROPOMI measurement (image). We use the created image patches to train a machine-learning classification model. The task of the model is to distinguish image patches with at least one ship from the image patches where there are no ships. The labels of the model were created using AIS ship location data, and, therefore, are independent of the distinctivity of ship plumes by a human. This way, the first research question we address in this study can be formulated as follows: **RQ1**: What is the minimum speed and

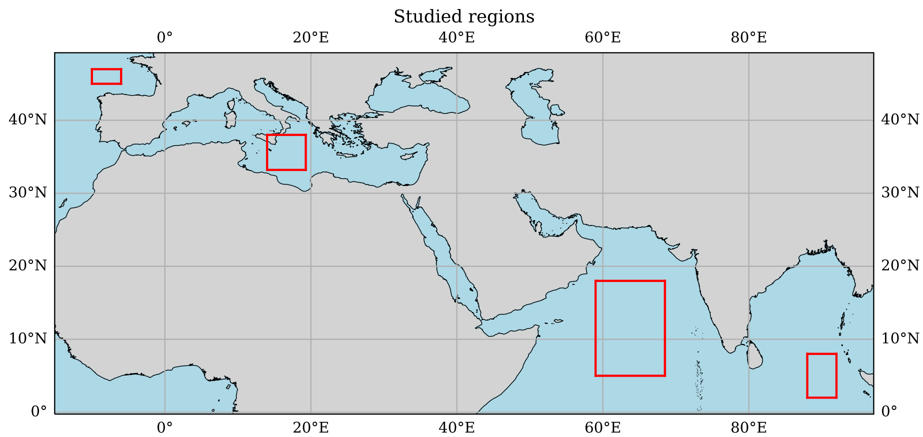

Figure 1: Red squares indicate bounding boxes of the four studied regions (from left to right): Biscay Bay, Mediterranean Sea, Arabian Sea, Bengal Bay.

length of a seagoing ship so that the NO_2 plume from it can be detected with the detection system using TROPOMI data? The second research question is as follows: **RQ2**: To what extent can the detectability of NO_2 plumes be improved if only the biggest emitters are taken into account? With the biggest emitters, we mean the biggest ships operating at the highest speeds, or several smaller or slower ships operating in proximity to each other. We then formulate the third research question of the paper. **RQ3**: Is there a potential for improvement of detectability of NO_2 plumes from the slow/small ships if more data is available?

The study is conducted on four regions of interest: Mediterranean Sea, Biscay Bay, Arabian Sea, and Bengal Bay (the coordinate scope see in Table 1 and Figure 1). The study areas are directed towards the Europe – Middle East – Asia trade route, with selected areas representing low background pollution and common occurrence of clear skies.

Region	Longitude [deg]	Latitude [deg]	Studied period
Mediterranean	(14, 19.3)	(33.2, 38)	(31-03-20; 28-02-23)
Biscay Bay	(-10, -6)	(45, 47)	(01-04-20; 28-02-23)
Arabian Sea	(59, 68.5)	(5, 18)	(31-03-20; 30-11-22)
Bengal Bay	(88, 92)	(2, 8)	(03-06-20; 31-12-22)

Table 1: Geographical coordinates and analyzed periods defining the study scope for each region.

The rest of the paper is organized as follows: In Section 2, we introduce the used data sources and explain how the data was pre-processed in order to obtain datasets used for machine learning models. In Section 3, we explain the experimental setup for each stage of the study and present the obtained results. We then present the discussion of the obtained results in Section 4, and conclude in Section 5.

2. Data

We create the dataset by combining the data from several sources: 1) the TROPOMI NO_2 measurements, 2) wind information, and 3) AIS (Automatic Identification System) data on ship positions. The dataset is prepared for supervised machine learning to identify image patches covering the area with a ship. With supervised learning, we aim to learn a function to predict the output for a feature vector. In our case, the output label of the function is the presence of a ship plume 'yes' – label equal 1, or 'no' – label 0. For the learning, pairs of feature vectors and corresponding output labels are given as a training set. In this Section, we describe all steps of the data preparation.

2.1. Data sources

Our main source of the data is the TROPOMI instrument. This is a UV-Vis-NIR-SWIR (UV, visible, near-infrared, short-wave infrared) spectrometer with the maximum ground pixel resolution of 3.5×5.5 km^2 at nadir. The TROPOMI instrument is on board the Sentinel-5P satellite mission – a sun-synchronous satellite with a local equatorial overpass time at 13:30. The TROPOMI instrument measures an extensive list of trace gases. In this study, we focus our attention on the NO_2 product[1]. Previous studies (Georgoulias et al., 2020; Kurchaba et al., 2021; Finch et al., 2022; Kurchaba et al., 2022, 2023) showed that with this data product, we can distinguish emission plumes from some individual seagoing ships. The NO_2 gas is a result of photochemical reactions of NO_x emitted by ships, which allows it to be used for ship emission monitoring. The trace gas variable of our interest is *Tropospheric Slant Column Density – SCD trop* (Eskes et al., 2022). In contrast to the commonly used *Vertical Column Density (VCD)*, in this study, we use *SCD trop* because we want to forego the use of the *airmass factor (AMF)* in the derivation process of the variable of interest. The *AMF* is calculated to convert satellite-observed *SCD*s of trace gases to *VCD*s. It accounts for the path length that sunlight travels through the atmosphere before reaching the satellite sensor, normalizing it by the amount of sunlight that would reach the surface under direct overhead conditions. However, the calculation of *AMF* to a large extent depends on the emission inventories and chemical transport models, which, in turn, rely on information about histor-

[1]TROPOMI Level 2 data version: 2.4.0.

ical concentrations of emissions, including NO_2 (Eskes et al., 2022). To avoid the potential impact of the historical data on the estimation of TROPOMI sensitivity, *SCD trop* will be used for the analysis presented in this study.

Information about wind speed and direction, which is crucial for understanding plume dispersion, is taken from wind speed data from the European Center for Medium-range Weather Forecast (ECMWF) at 10 m height, available with 0.25° resolution at a 6-hourly time step. The data is available as a support product in a TROPOMI file.

The used data on ship positions comes from Automatic Identification System (AIS) transponders. As of 2002, all commercial sea-going vessels are required to carry an onboard AIS transponder (Mou et al., 2010). Among others, the data include the position, speed, and unique identifier (MMSI) of each ship carrying an active transponder. Information about the dimensions of the ships is obtained from the official ship registries. Since at the moment there is no open-access AIS data available, for the scope of this study, the AIS data, as well as information about the dimensions of the ships, were provided by the Netherlands Human Environment and Transport Inspectorate (ILT) – a partner of this research.

2.2. Data preprocessing

The first step of data preparation is regridding[2]. This is done so that for each region we have pixels with the same spatial coverage. The regridded pixel size for each region is approximately equal to 4×5 km^2. Following the set-up used in the previous studies (Kurchaba et al., 2022, 2023), for the

[2]The regridding is performed using the Python package HARP v.1.13.

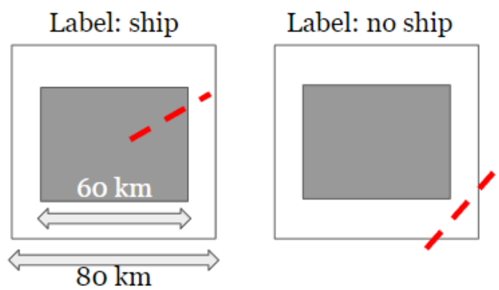

Figure 2: An illustration of the set-up used for counting the number of ships per image patch. White square – image patch. Black square – a central part of the image patch. Red dashed lines – an example of ship trajectory starting from 2 hours before until the moment of the satellite overpass. Only ships, whose trajectories cross the central part of the image patch are considered to be present in the area covered by a patch.

regridding, we only use pixels with cloud coverage below 0.5, wind speed lower than 10 m/s, and *qa value* above 0.5 (Sneep, 2021). This level of qa value filtering was shown to be sufficient for the identification of NO_2 plumes from individual ships and is a trade-off between a high standard of data quality, and an attempt to preserve as many data points as possible. In the Appendix A, the reader can find an assessment of the data loss in case *qa value* filtering was set to the level of 0.75 – the level suggested in the TROPOMI manual (Eskes et al., 2022).

As a next step, we split the studied area into non-overlapping patches of 80×80 km^2. The selected size of the image patch corresponds to a distance that the fastest ships in the dataset will cover in 2 hours. The observation period of 2 hours was motivated by the fact that due to the physical dispersion and limited lifetime of NO_2 within plumes, the detectability of ship plumes will fall sharply after 2 hours (Vinken et al., 2011). For each image patch, we calculated how many ships were in the central area of the patch within

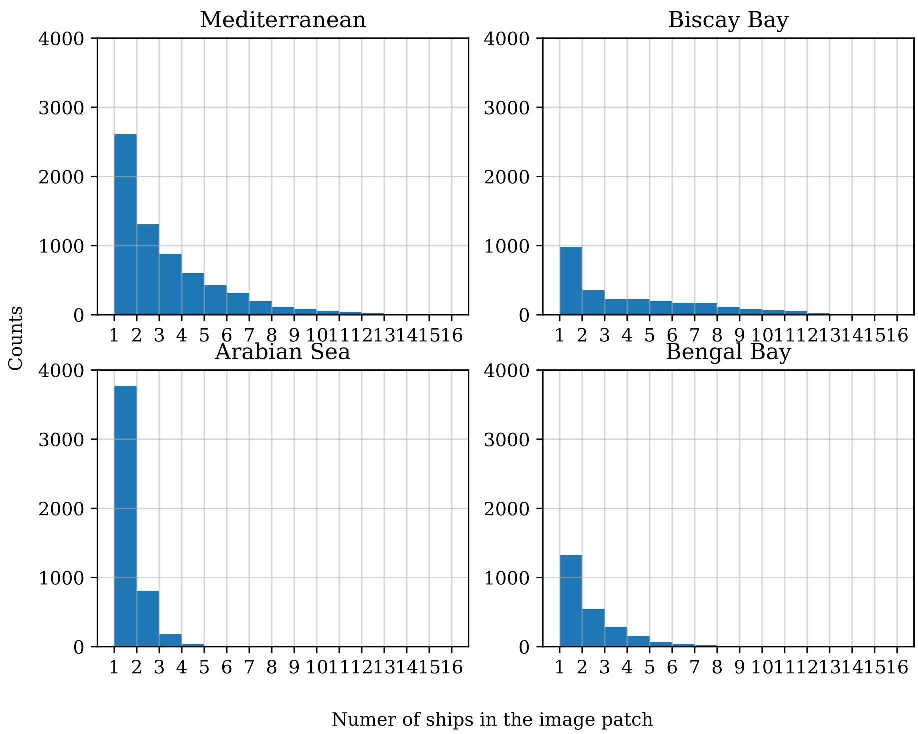

Figure 3: Distribution of ship number per image patch for the studied regions.

Region	Ship image	No ship image
Mediterranean	6652	9693
Biscay Bay	2641	2812
Arabian Sea	4804	24594
Bengal Bay	2444	6848

Table 2: Class-wise distribution of image patches for each studied region. The rate of imbalance depends on the traffic density in the region.

2 hours before the overpass of the satellite. The central area of the patch is defined as a 60×60 km^2 square. We do not take into account ships that do not pass through the central area of the image patch, as the probability that their plume will be located within the image patch is very low. An example is presented in Figure 2. The resulting distribution of the number of ships per image patch for each studied region can be found in Figure 3. Please note the regional differences in the distribution of ships among patches. The Arab Sea typically has a high number of patches with a single ship. The Biscay Bay, in comparison to other regions, has the highest number of patches with a high number of ships in it. These patterns illustrate the differences in shipping density among the studied regions.

2.3. Preparation of the dataset

To study the sensitivity of the TROPOMI satellite with respect to the detection of NO_2 plumes from seagoing ships, we prepare a dataset for supervised machine learning. The objective is to distinguish image patches that cover the area where there was no ship, from image patches covering the area

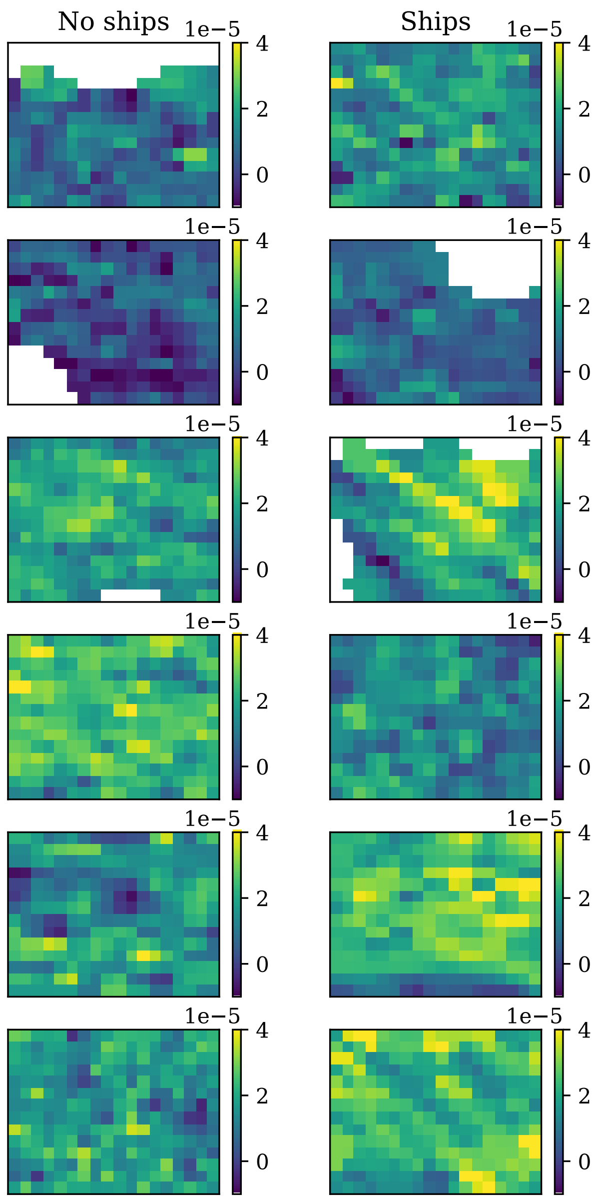

Figure 4: Examples of image patches without a ship and with at least one ship on it. The presented image patches were randomly sampled from the dataset of the region Biscay Bay. Not all images of the second column contain a ship plume, which means that ships present in the area covered by a patch are likely to be below the sensitivity limit of the TROPOMI instrument.

with at least one ship on it. Since this is a binary problem, the value of the output label is 1, if there is at least one ship that is faster than 6 kt, which is approximately 11.1 km/h and longer than 90 m in the area covered by an image patch. The output label is 0, if there is no ship in the area, or the ship is shorter than 90 m or slower than 6 kt. The values of 90 m and 6 kt are sufficiently low to be well below detectable limits as will also follow from this study. Table 2 shows the resulting distribution of classes for studied regions. Examples of image patches without (label 0) and with at least one ship on it (label 1) are presented in Figure 4. We can see that not all image patches with a ship actually contain a visually distinguishable plume. This is because the NO_2 plumes produced by some ships are below the sensitivity limit of the TROPOMI instrument, or we are not able to distinguish it visually.

We address the classification problem with a multivariate classifier. Therefore, we represent the TROPOMI image patches in terms of a set of features - a statistical representation of the image patch. For the regridded pixels of each image patch, we calculate the following statistics: *min(SCD), mean(SCD), median(SCD), max(SCD), std(SCD)*, where SCD stands for NO_2 slant column density. To give information about the level of plume dispersion, we add wind-related variables *zonal wind velocity (wind zon), meridional wind velocity (wind med)*, which represent the speed of the wind from the west to east and from south to north respectively. Finally, we add features *sensor zenith angle, solar zenith angle* and *solar azimuth angle* to represent the viewing geometry of the satellite. Values for wind information and satellite geometry are the average values of the pixels within the image patch. The resulting feature set is presented in Table 3. In Appendix B, the reader can find histograms of the dataset features for the studied regions. Clearly, the features related to the properties of ships cannot be included in the feature space, because the presence of a ship has to be established. Moreover, we deliberately do not include any features in the feature set related to the geographic locations of a given patch. This is because shipping lanes may bias the model. The dataset used in this study as well as the code used for generating the presented in this study results are available publicly as a reproducibility capsule (Kurchaba et al., 2024). Prior application of a machine learning model, all features were standardized using a median-interquartile range scaling[3] – a scaling technique that allows to reduce a negative impact of the outliers in the dataset (Fabian, 2011).

3. Experiments and results

In this Section, we describe the experiments and show the results obtained. We start with introducing the classification model – we present model selection and hyperparameter optimization results. For the selected model, we provide the explainability analysis. Next, in the consecutive subsections, we explain and provide the results of the experiments addressing the three research questions of this study.

3.1. Classification model

3.1.1. Experimental setup

As a first step, we compared the performance of several multivariate classifiers and selected the one that is going to be used in the remaining part

[3]RobustScaler implemented in scikit-learn v.1.2.2.

Feature type	**Feature name**
NO_2 slant column density	min(SCD)
	mean(SCD)
	median(SCD)
	max(SCD)
	std(SCD)
Wind information	zonal wind velocity
	meridional wind velocity
Satellite geometry	sensor zenith angle
	solar zenith angle
	solar azimuth angle

Table 3: List of features used for classification model.

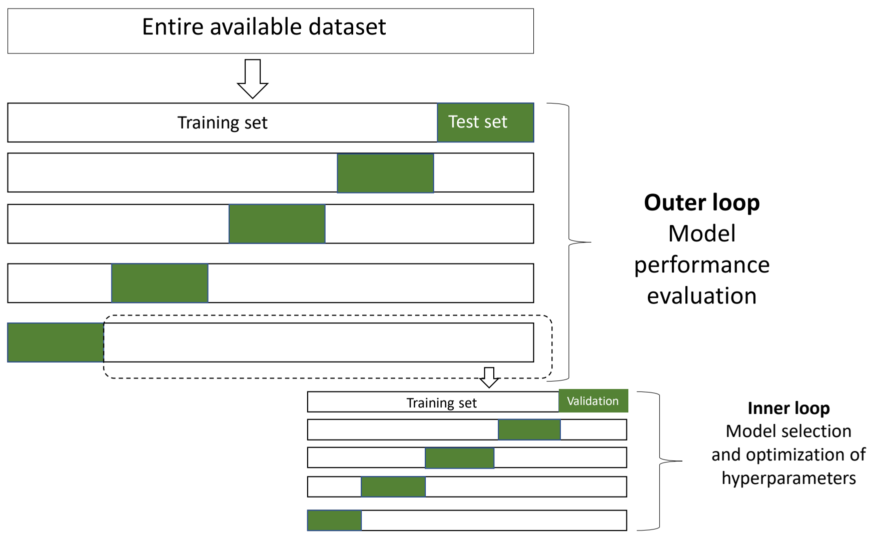

Figure 5: Nested cross-validation. Applied scheme of hyperparameter optimization and model selection. Source: (Kurchaba et al., 2023).

of the paper for the sensitivity analysis. We studied four machine learning classifiers of increasing complexity: Logistic regression, Support Vector Machine (SVM) with the radial basis function (rbf) kernel, Random Forest[4], and Extreme Gradient Boosting[5] (XGB) (Chen and Guestrin, 2016). All selected models are robust to noise and can be efficient even given the relatively small size of datasets. To make sure that we exploit the maximum potential of a given machine learning model, we optimized the hyperparameters of each studied model. The hyperparameters were optimized using a random search[6] technique with the objective metrics - *average precision*. The

[4]All above-mentioned models are implemented in Python scikit-learn v.1.2.2.
[5]XGBoost v. 1.7.0
[6]Implemented in Python scikit-learn v.1.2.2.

used search space of the hyperparameters for each of the studied models is provided in Appendix C. To be able to simultaneously perform the hyperparameter optimization and evaluation of the model performance, we used 5-fold nested cross-validation (Stone, 1974; Cawley and Talbot, 2010). The general setup of nested cross-validation is as follows: In the outer loop of cross-validation, the entire dataset is split into K subsets (folds). Since we applied 5-fold cross-validation, in our case, $K = 5$. The model is trained on K-1 subsets, while the remaining subset is used for the model evaluation. This procedure is repeated K times. Within each iteration of the outer loop, an inner cross-validation loop is performed. The training data from the outer loop is further split into K-1 subset for training and one subset for validation. Different model hyperparameters are tested using the training and validation sets in the inner loop. The model with the best performance on the inner loop validation set is selected. The selected model from the inner loop is then evaluated on the test set from the outer loop. For visual explanation, see Figure 5. To maintain the same percentage of samples of a certain label in the training and test set, the cross-validation was based on *stratified K-fold* splits (Hastie et al., 2009; Géron, 2022). The set of hyperparameters yielding the best results at each iteration of cross-validation is provided in Appendix D. The metrics used for models' performance evaluation were *precision-recall curve* – a curve depicting precision as a function of recall (explanation of the terms is provided below), *average precision* – the area under the *precision-recall curve*, the *Receiver Operating Curve (ROC)* – curve visualizes True Positive Rates as a function of False Positive Rates, and the *Area Under the Receiver Operating Curve (ROC-AUC)*. We defined the above-mentioned terms as follows:

$$Precision = \frac{TP}{TP + FP} \quad (1)$$

$$Recall = True\,positive\,rate = \frac{TP}{TP + FN}, \quad (2)$$

$$False\,positive\,rate = \frac{FP}{FP + TN}, \quad (3)$$

where TP stands for true positives and corresponds to the image patches with a ship, which were correctly identified by the classifier. FP – false positives correspond to image patches covering an area without any ship, but that were identified by a classifier as ones with a ship. FN stands for false negatives and corresponds to image patches that were not classified as a patch with a ship but, in fact, were covering an area with a ship on it.

3.1.2. Results

The classification results are presented in Table 4. Comparing the performances between different classifiers, we can see that the XGB classifier yielded the best results for most of the regions – we used this classifier for the remaining experiments of this study. Comparing the results between regions, we start with ROC-AUC. The highest achievable score of ROC-AUC is equal to 1. While the ROC-AUC score that will be obtained in case of random guessing is 0.5. The ROC-AUC score is calculated based on the ROC curve. For the XGB classifier, it is presented in the right-hand side plot of Figure 6. The scores for Biscay Bay and the Mediterranean Sea are higher

Region	**Model**	**Average Precision**	**ROC-AUC**
Mediterranean	XGB	**0.636 ± 0.013**	**0.712 ± 0.011**
	Random Forest	0.629 ± 0.018	0.706 ± 0.016
	SVM (rbf)	0.615 ± 0.015	0.694 ± 0.013
	Logistic	0.448 ± 0.008	0.546 ± 0.009
Biscay Bay	XGB	**0.704 ± 0.021**	**0.713 ± 0.015**
	Random Forest	0.620 ± 0.025	0.652 ± 0.022
	SVM (rbf)	0.573 ± 0.020	0.589 ± 0.014
	Logistic	0.523 ± 0.013	0.541 ± 0.018
Arabian Sea	XGB	0.226 ± 0.007	0.610 ± 0.008
	Random Forest	**0.229 ± 0.006**	**0.618 ± 0.006**
	SVM (rbf)	0.195 ± 0.004	0.545 ± 0.007
	Logistic	0.169 ± 0.003	0.498± 0.008
Bengal Bay	XGB	**0.379 ± 0.017**	**0.601 ± 0.01**
	Random Forest	0.364 ± 0.016	0.601 ± 0.010
	SVM (rbf)	0.346 ± 0.006	0.560 ± 0.016
	Logistic	0.289 ± 0.015	0.542 ± 0.016

Table 4: Results of the optimization of the classification models' hyperparameter. The reported results were obtained on the hold-out test sets based on nested 5-fold cross-validation (Stone, 1974; Cawley and Talbot, 2010). The bold font indicates the performance of the best model for a given region.

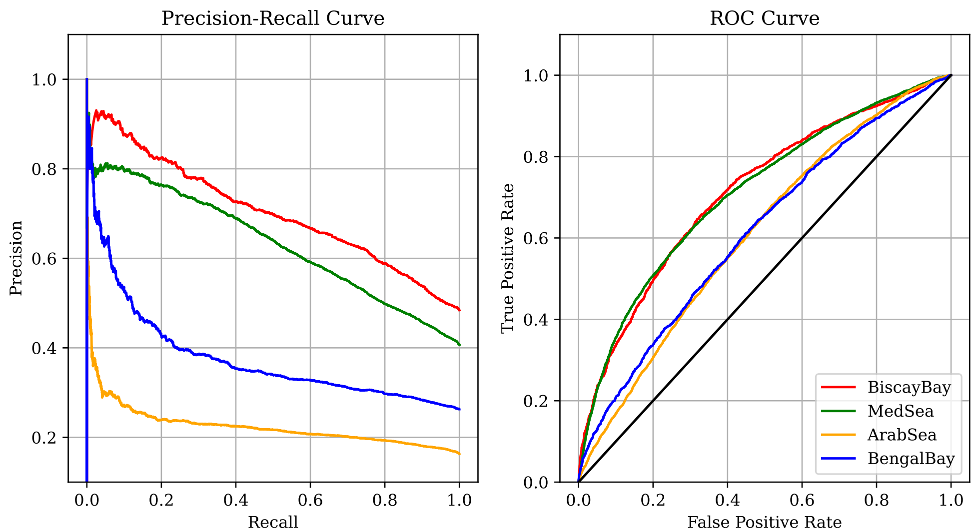

Figure 6: Precision-recall and ROC curves for the studied regions. The black line in the right panel – performance of a random guess classifier.

than for the Arabian Sea and Bengal Bay. One of the reasons for this difference might be that the regions Biscay Bay and the Mediterranean Sea have a higher overall number of ships per image patch (and, therefore, a higher percentage of potentially well-recognizable plumes) than the two remaining regions, c.f. Figure 3. Next, we compare the scores of average precision. Also in the case of this metric, a perfect classifier would have a score of 1.0, while a random guess classifier would have an average precision score equal to the ratio of positive samples in the dataset. The average precision score is calculated based on a precision-recall curve, which is presented in Figure 6, left-hand-side plot. Due to the different rates of class imbalance of datasets from different regions, the average precision scores from the Table are difficult to compare directly. However, analyzing the precision recall-curves, we can conclude the following: the performance of the classifiers on Biscay Bay and Mediterranean Sea regions are very close to each other and the difference between the obtained average precision scores is mainly caused by a slightly different class imbalance. The lower average-precision scores for the regions Bengal Bay and Arabian Sea are also to a big extent a result of the fact that those datasets contain fewer image patches with a ship than two other regions. However, in the case of Bengal Bay, for the lower rates of recall, we can observe quite high values of precision. This signalizes the fact that there is a set of images that the model can quite confidently correctly recognize. This is not the case for the Arabian Sea, which implies better performance of the classification model on the Bengal Bay region in comparison to the Arabian Sea. For all regions, it is important to underline that the reported performances of the models were negatively affected by the presence of ships whose size and speed are known to be too small or slow to be detected by the TROPOMI instrument, which is a cause of the topic of this research, that is the study of the detection limits.

3.1.3. Explainability analysis

As a next step, we would like to understand which of the used features are the strongest indicators of the presence of a ship in the area for the XGB model. For this, we perform the explainability analysis using the SHapley Additive exPlanations (SHAP) (Lundberg and Lee, 2017) summary plots (see Figure 7). The plots indicate the strength of the impact of a value of a certain model feature on the model outcome (positive or negative) for individual samples from the test set. The red and blue colors show the effects of a certain feature's high and low values respectively.

We can see that for the Mediterranean Sea, and Biscay Bay, the fea-

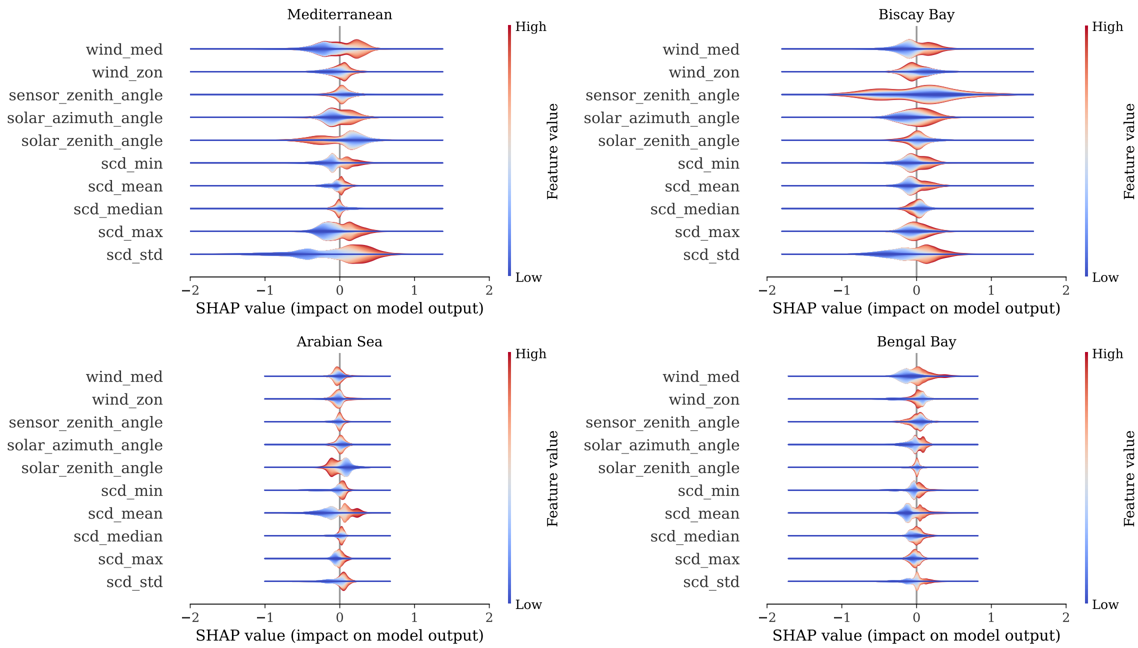

Figure 7: SHAP violin plots on concatenated test sets for each studied region.

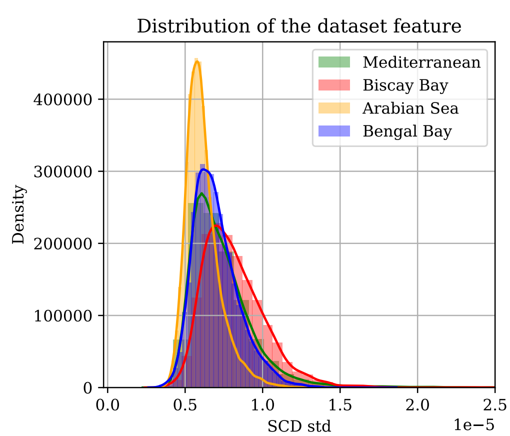

Figure 8: Distribution of the variable *scd std* for four studied regions. For the Arabian Sea, the distribution is noticeably more narrow than for other regions.

ture having the strongest impact on the decision of the model the most is *scd std*, representing the standard deviation of stratospheric column density within the image patch. In the case of the Mediterranean Sea, *scd max* and *solar zenith angle* also play significant roles. Interestingly, the direction of the meridional wind also has a strong influence on the model's decision in the Mediterranean Sea. From the plot, we see that the negative meridional wind corresponds to strong negative model responses, potentially due to land outflow from Europe affecting ship plume visibility. In the Arabian Sea and Bengal Bay regions, the strongest impact on the model response is attributed to the values of the feature *scd mean*. Notably, for the Arabian Sea, high values of *scd std* do not necessarily indicate the presence of a plume, possibly because as we can see from Figure 8, standard deviations of NO_2 concentrations in this region are typically lower compared to others. Low values of *scd std*, however, are used by the model as a strong suggestion of the absence of a plume in the image patch. Finally, one can notice that for Biscay Bay, the feature *sensor zenith angle* is of great importance. However, since we do not see a clear split into high/low values for positive/negative model outcomes, the influence of the feature on the model response will depend on the values of other features (Friedman and Popescu, 2008; Hastie et al., 2009). From this experiment, we can conclude that the same machine learning models applied to different studied regions not only yield different quality of results but are also driven by different sets of features.

3.2. RQ1: Sensitivity limits estimation

3.2.1. Ship emission proxy – definition

In this Subsection, we address the first research question: What is the minimum speed and length of a seagoing ship so that the NO_2 plume from it can be detected with the detection system based on TROPOMI data? With the detection system we mean a sequence of steps needed to automatically detect an NO_2 plume from a ship on a TROPOMI image patch. The first step of this sequence is a measurement performed by the TROPOMI sensor. The last step is the application of a trained machine-learning model on the set of unseen image patches with the aim of distinguishing patches covering the area with a ship. In (Georgoulias et al., 2020), it was shown that the length and the speed of the ship are the main factors determining the emission potential of the ship. Following the considerations presented in (Georgoulias et al., 2020), in order to decrease the level of problem complexity, we represent the speed and length of the studied ship in terms of one variable – the ship emission proxy E_s (Georgoulias et al., 2020) defined as:

$$E_s = L_s^2 \cdot u_s^3 \tag{4}$$

where L_s is the length of the ship in m and u_s is the speed of the ship in m/s. If there is more than one ship in the area covered by the image patch, the total emission proxy is computed as the sum of the E_s for all ships in this area. For the purpose of this paper, we define the sensitivity limit of the detection system for NO_2 plumes from seagoing ships using TROPOMI data for a given region as the level of ship emission proxy E_s, starting from which the classification model can distinguish image patches without a ship from image patches with a ship.

Region	Average Precision	ROC-AUC
Mediterranean	0.538 ± 0.036	0.518 ± 0.038
Biscay Bay	0.539 ± 0.053	0.513 ± 0.067
Arabian Sea	0.563 ± 0.035	0.560 ± 0.031
Bengal Bay	0.564 ± 0.054	0.540 ± 0.060

Table 5: Model performance when only considering the one-ship patches with the emission proxy below 10% quantile.

3.2.2. The lowest emitters in the dataset

Given the provided definition of the sensitivity limit, our initial investigation evaluates the classification model's performance using image patches with the lowest total emission proxy. For this, we first exclusively chose patches covering a single ship. Then, from the selected subset, we further narrowed our selection to those patches with an emission proxy falling below the 10% quantile of all one-ship patches.

To ensure comparability of performance metrics between areas and samples with different ship proxy values, we took a sample with an equal number of patches with and without a ship covered by the patch. To make sure that all image patches with and without ships that satisfy the above-provided criteria are used for the model training and evaluation, we repeated the sampling procedure 5 times. Subsequently, we conducted a 5-fold cross-validation for each set of sampled data points. The averaged results over the five folds are presented in Table 5.

The outcomes indicate that none of the regions allowed for distinguishing

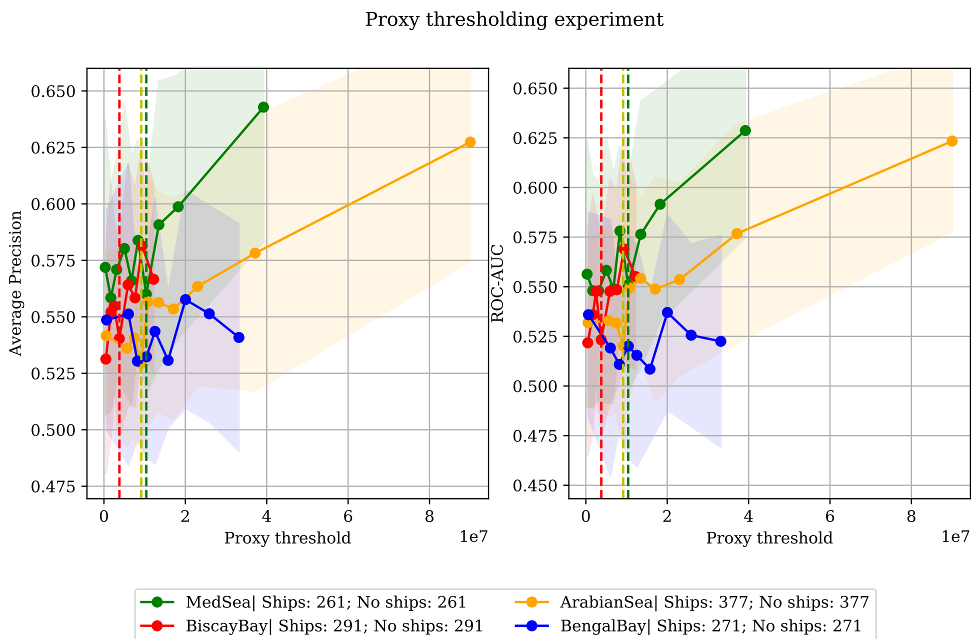

Figure 9: Step-wise removal of the patches (containing one ship) with the lowest emission proxy. Dashed lines indicate estimated levels of sensitivity limits for the Biscay Bay, Mediterranean, and Arabian Seas. To assure the comparability of the results, a similar size of training/test datasets was used at each threshold level.

patches with a ship, as the ROC-AUC/Average precision values obtained were not significantly higher than 0.5. Consequently, we infer that the ships with the lowest emission proxies in our dataset fall below the sensitivity limit of the detection system for NO_2 plumes from seagoing ships using TROPOMI data.

3.2.3. On sensitivity limits of TROPOMI data-based detection system

In the next experiment, we checked what the emission proxy threshold for the ship plumes detectability is. Here, we again considered only image patches with one ship on it. We then gradually removed ships with the lowest emission proxy from the dataset, analyzing the changes in the model performance.

The applied emission proxy thresholds were determined as a range of quantiles starting from 10% and gradually increasing by 10%, until it reaches 90%. If after reaching a certain level of threshold, the number of patches with a ship (label 1) went below 300, the experiment was terminated and the next thresholding levels were not tested[7]. The criterion of 300 patches was established based on the number of patches with a ship left after a 90% threshold applied for the region with the highest number of one-ship patches available (Arabian Sea).

Clearly, by removing the image patches with the proxy values below a certain threshold, we decreased the size of the dataset. To eliminate the potential effect of the dataset size on the model performance, throughout the experiment, we kept the dataset size constant. To achieve this, for each applied threshold, we sampled the number of data points equal to the number of data points available for the highest applied threshold. As in the previous experiment, we repeated the sampling procedure 5 times. For each set of sampled data points, we performed a 5-fold cross-validation.

The results of the experiment are presented in Figure 9. We can see that for the lowest thresholds, for all four regions, the average performance quality did not change. This means that the removed ships were still below the sensitivity level of the detection system for NO_2 plumes from seagoing ships using TROPOMI data. From a certain threshold (indicated with dashed

[7]This way, the highest applied threshold for Biscay Bay was 70% and for Bengal Bay 80% quantile.

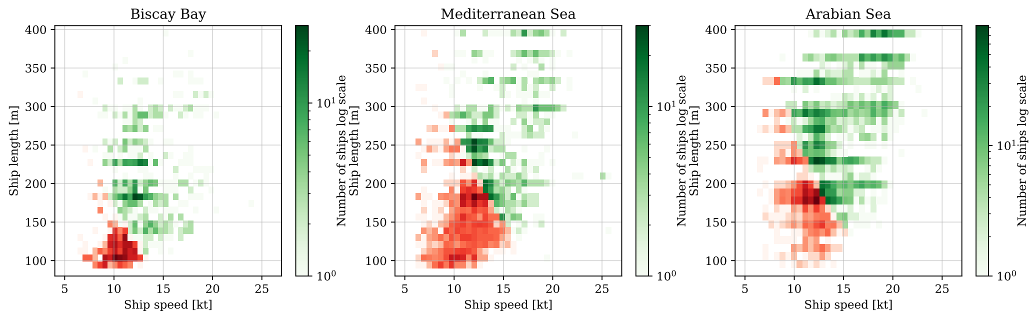

Figure 10: 2D histograms of speed and lengths for ships that are above (green) and below (red) the estimated sensitivity limits for the Biscay Bay, Mediterranean, and Arabian Seas.

lines on the plot), however, the model performance started to increase. The level of the ship emission proxy threshold starting from which we observe the improvement of the performance of the model is the sensitivity limit of the detection system for NO_2 plumes from seagoing ships using TROPOMI data for a given region. For the Mediterranean and the Arabian Sea, the sensitivity limit in terms of ship emission proxy was established to be around $1 \times 10^7 m^5/s^3$. For the Biscay Bay, the sensitivity limit is lower and is around $3.8 \times 10^6 m^5/s^3$. To get the intuition around these numbers, we return to the values of speed and length of the ship. To achieve this, for the regions of the Biscay Bay, Arabian, and Mediterranean Seas, in Figure 10, we present 2D histograms of the speed and length of ships that are above (green color) and below (red color) the estimated sensitivity limits. From the histograms, we conclude that to distinguish NO_2 plumes, the minimum speed of the ship for the Arabian and Mediterranean Seas should range between 10 and 15 kt depending on the length of the ship. Ships that are slower than 10 kt or shorter than 150 m are below the sensitivity limit. For the Biscay Bay, the limit lies around 8 kt and 100 m. For Bengal Bay, the sensitivity limit cannot be determined since the available amount of data did not allow us to raise the proxy threshold high enough to see the increase in the performance of the model. However, when comparing the curve dynamics of the Bengal Bay with other regions, the obtained pattern suggests that the sensitivity limit for this region is higher than for the Arabian and Mediterranean Seas.

3.3. RQ2: On detection of the biggest emitters

Our second research question is how the detectability of NO_2 plumes can be improved if only the biggest emitters are taken into account. Our aim here is to understand the potential of the detectability of NO_2 plumes when the total emission proxy is very high. The high emission proxy can result from a big ship operating at a high speed, or smaller or slower ships operating in proximity to each other. Therefore, in this experiment, we considered all image patches (without, with one, or with more than one ship on it). This way, in some of the image patches, there will be more than one ship with a high emission proxy present.

As in the previous experiment, we gradually removed from the dataset the image patches with the lowest total emission proxy. Once again we studied how the removal of the low emitters affects the quality of classification. The thresholds used for the proxy filtering were determined as quantiles of the proxy values of the dataset of a given region. For the Mediterranean and Arabian Sea, the applied quantiles ranged from 0 to 90%. For the Biscay and Bengal Bay, due to the smaller sizes of the datasets, the applied quantiles ranged from 0 to 80%.

In Figure 11, we present the results of the experiment. For each of the studied regions, we can observe an increase in the model performances. We

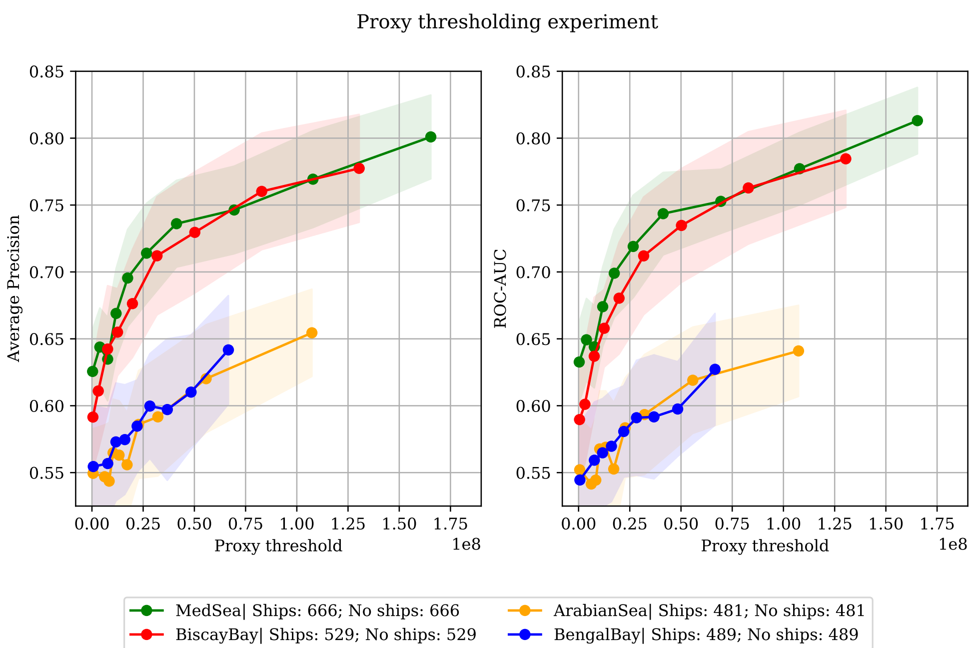

Figure 11: Illustration on how the step-wise removal of the image patches with the lowest total emission proxy from the dataset affects the performance of the classification model.

can see that for the Mediterranean Sea, for the patches with the highest total emission proxy, the ROC-AUC score can exceed 0.8. For the regions Arabian Sea and Bengal Bay, the level of the results is noticeably lower. This pattern in the results is similar to what we observed in Subsection 3.1.

As a next step, we checked if the dependency between the applied proxy threshold and classification performance is impacted by a certain hyperparameter configuration of the XGB model. We would like to know to which extent we can improve the quality of classification for the image patches with the highest total emission proxy. For this, we studied two configurations of the dataset. In the first case, we applied the highest proxy threshold for the given region (the last data point from the corresponding plots of Figure 11). In the second case, we did not apply any proxy threshold but kept the dataset size equal to the case when the proxy threshold was applied (the scenario corresponds to the first data point of the corresponding plots of Figure 11). For each of the datasets, we performed optimization of the hyperparameters of the classification model, in the same way as it is explained in 3.1. We then compared the performance of the models for both scenarios. The results are presented in Figure 12. For all studied regions, we can see that the quality of detecting NO_2 plumes from ships can be improved if only the image patches with the highest total emission proxy are considered. Based on this, we conclude that the dependencies shown in Figure 11 are not the results of a particular model configuration, but rather a property of data. However, we can see that the optimization of the hyperparameters of the model did not result in the improvement of the model performance.

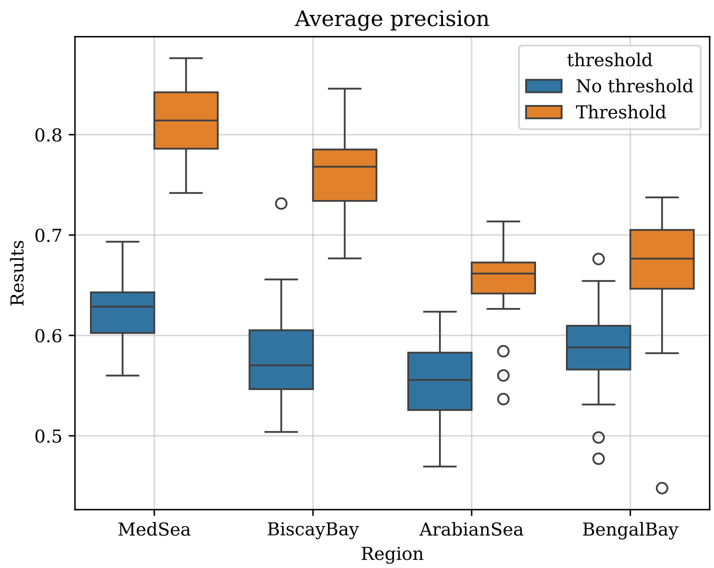

(a)

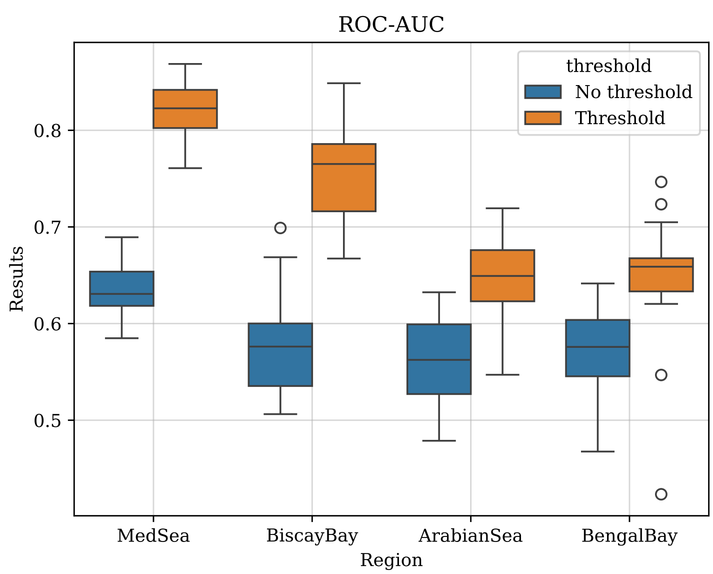

(b)

Figure 12: Comparison of the performance of the model when all ship images are in the dataset and when only images with the proxy above the predetermined proxy threshold are used.

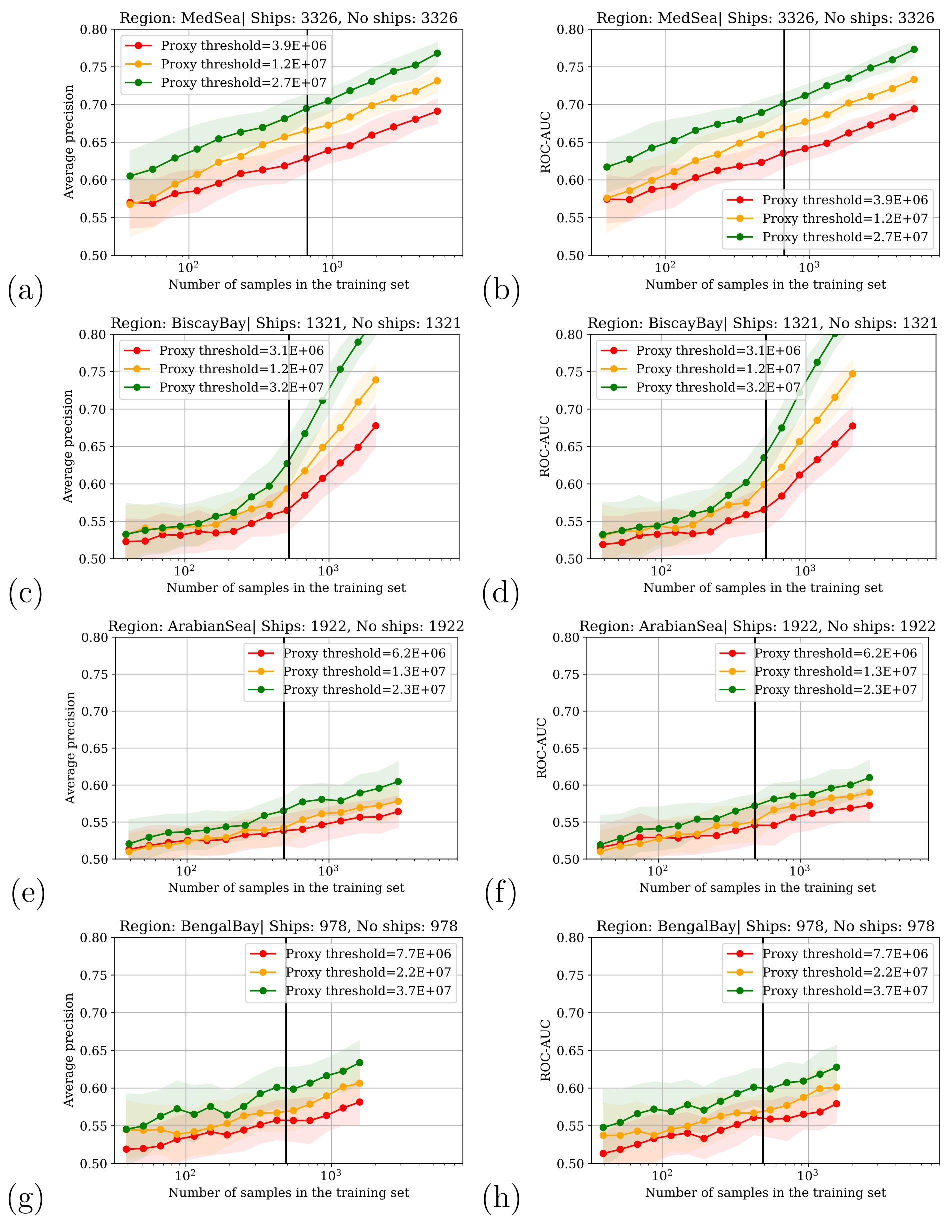

Figure 13: Learning curves for different levels of the applied thresholds. The black line indicates the dataset size that was used for the experiments reported in Figures 11, 12.

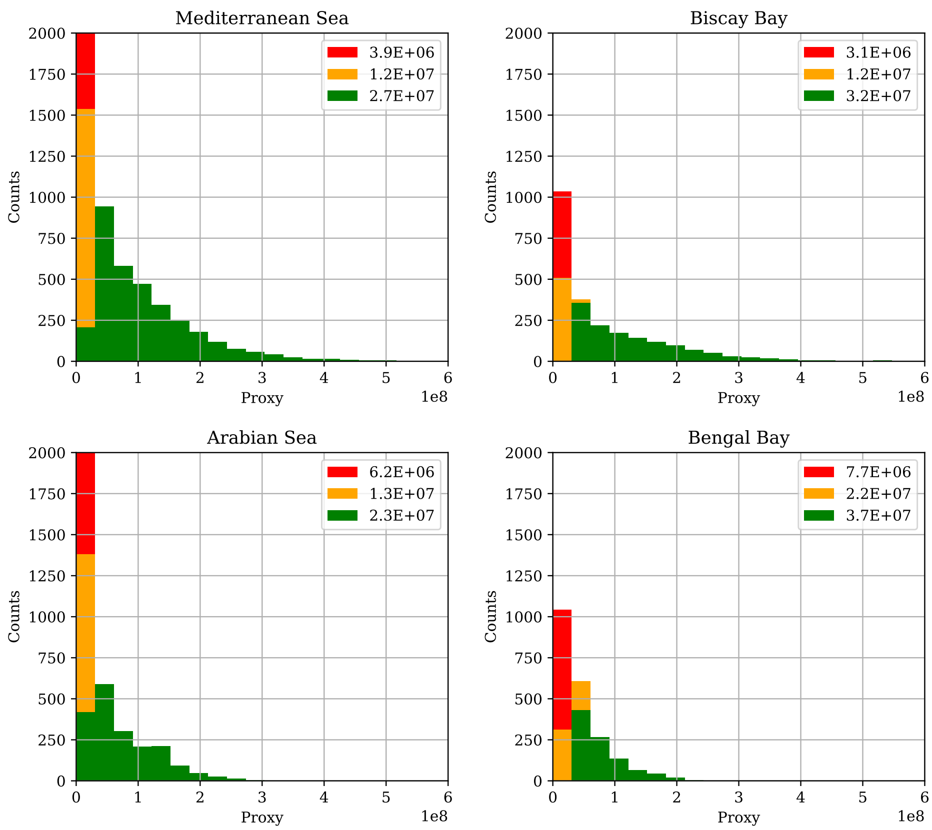

Figure 14: Change of the ship proxy distribution after applying thresholds as in Figure 13.

3.4. RQ3: On potential improvement of small ship detectability

In this Subsection, we address the third research question of the study. Namely, we investigate whether there is a potential for improvement of detectability of NO_2 plumes from the slow/small ships if more data would be used for the training of the classification model. For each region, we selected three proxy thresholding levels and studied the change in the model performance with the growth of the size of the dataset used for the model training. We focus here on the low thresholds. The used thresholds were set as 10%, 30%, and 50% quantiles of the proxy value for the Mediterranean Sea and Biscay Bay. For the Arab Sea and Bengal Bay, the applied thresholds were 10%, 40%, and 60% due to the fact that the model performances on the lowest quantiles were indistinguishable. Similarly to the previous experiment, the maximum size of the dataset was defined by the number of data points in the dataset with the proxy value higher than the highest among the three applied thresholds.

The resulting learning curves for each of the studied regions are presented in Figure 13. We can see that for all studied regions, the results shown in Figure 11 can be improved by using more data for model training. We also observe that for the regions Biscay Bay and Mediterranean Sea, more data results in a more significant increase in performance, than for the Arabian Sea and Bengal Bay. To explain this, in Figure 14, we present the distribution of the variable ship emission *Proxy* for each consecutive threshold applied. The histograms show that for the Biscay Bay and the Mediterranean Sea, there are many more image patches with high values of total emission proxy than for the Arabian Sea and Bengal Bay. As a result, even after removing from the dataset the image patches with the lowest total emission proxy, for such regions as the Arabian and Bengal Bay, the models are still trained on significantly lower total emission proxies than the models for the Biscay Bay and the Mediterranean Sea.

4. Discussion

The main objective of this study was to investigate the sensitivity limits of a detection system for NO_2 plumes from seagoing ships using TROPOMI data, considering the speed and length of the ships that we expressed through the means of ship emission proxy. By the detection system, we mean a sequence of steps starting from the signal measurement by the sensor, followed by data retrieval, and finally the application of the developed methodology of automated detection of ship plumes. Each of these steps influences the numbers obtained in this study.

To be able to address the problem of sensitivity estimation, we build a methodology based on machine-learning classification models. This approach allowed us to effectively exploit the TROPOMI signal and contextual information while automatically separating the image patches into those, where the NO_2 plumes can and cannot be detected. The choice of a multivariate model enabled us to take into account features important for satellite sensitivity, such as wind and satellite/solar viewing angles. Studying several machine learning classifiers of increasing complexity, we found that the XGB model yielded the best performance across most regions. This shows the importance of the application of complex machine-learning models for the effective identification of TROPOMI image patches with NO_2 plumes from ships with a relatively low number of features.

4.0.1. RQ1

With the first research question, we attempted to determine the minimum speed and length of seagoing ships for which the TROPOMI data-based detection system can detect NO_2 plumes. We first showed that while the smallest ships considered in our dataset are below the detection limit of the system, once reaching a certain level of ship speed/size, the signal becomes detectable. Second, for the Mediterranean Sea and the Arabian Sea, we estimated sensitivity limits of approximately $1 \times 10^7 m^5/s^3$. For Biscay Bay, the obtained limit lies around $3.8 \times 10^6 m^5/s^3$. Comparing the obtained numbers with the ship emission estimation provided in (Georgoulias et al., 2020), we can see that our detection system allows us to correctly recognize some plumes with concentrations close to the background concentrations estimated for the Mediterranean Sea. The obtained values of emission proxy translate to the minimum detectable speed of 10 kt and minimum detectable length of 150 m for the Mediterranean and Arabian Seas and 8 kt and 100 m for Biscay Bay. Comparing those numbers with speed and length thresholds used in previous studies, we can see that previously applied thresholds were put higher than the actual possible detection limits. Unfortunately, due to the insufficient amount of data, the sensitivity limits for the Bengal Bay region could not be determined.

4.0.2. RQ2

With the second research question, we examined the potential improvement in NO_2 plume detectability when considering only the biggest emitters.

With our results, we numerically confirmed that restricting the analysis to faster/larger ships leads to enhanced detectability of NO_2 plumes. For the Mediterranean Sea region, the performance of the classification model can exceed 0.8 ROC-AUC and average precision scores. This finding suggests concentrating the focus on the larger emitters, could potentially increase the efficiency of the application and accuracy of ship emission monitoring using the TROPOMI instrument. Our analysis also revealed distinct differences in model performance quality between regions. Notably, the Mediterranean Sea and Biscay Bay consistently show better performance compared to the Arabian Sea and Bengal Bay. We can see that these variations could be attributed to variations in ship traffic density between the regions. Additional factors that potentially can influence the performances of the models are measurement conditions (e.g., number of cloudy days), differences in data quality between regions (c.f. Table A.6), and different scales of temperature fluctuations or concentration of ozone in the background. The last two factors affect the lifetime of NO_2. However, an in-depth understanding of this problem requires a separate study and we leave it as future work.

4.0.3. RQ3

Our investigation into the third research question, regarding the potential for improving NO_2 plume detectability from slow or small ships by utilizing more training data, again showed the variability of the results across the regions. For the Mediterranean Sea and Biscay Bay regions, an increase in data volume led to a notable enhancement in model performance. While, for the Arabian Sea and Bengal Bay, the impact of increased data, even though present, was less pronounced. One of the established reasons was the fact that for European regions we had a higher ratio of data points with a high value of emission proxy in the dataset than for the Bengal Bay and Arabian Sea. Nevertheless, the obtained results indicate that the accuracy of currently determined detection limits is perhaps constrained not by the methodology or the sensor, but by data availability.

4.0.4. Implications and future work

The insights gained from this study have important implications for satellite-based ship emission monitoring. By identifying sensitivity limits and optimal ship characteristics for detectability, our findings guide the scope of future studies on ship's NO_2 estimation using TROPOMI data and give an overview of the potential application of the TROPOMI instrument for ship emission monitoring. Moreover, the obtained results can be used as a benchmark sensitivity level for future satellite missions, such as, for instance, TANGO (Landgraf et al., 2020).

In future research, it would be valuable to explore factors beyond ship speed and length that influence detectability, such as temperature regimes, clouds, background ozone concentrations, effect of the sunglint or satellite viewing angle. Moreover, it would be valuable to perform an in-depth study explaining the observed multi-regional differences in ship plume detectability. Finally, studying different types of machine-learning architectures or including more data features in the used datasets can provide additional insights into understanding if the ship plume detectability limits can be lowered further by means of potential improvement information extraction from image patches. A possible candidate is Convolutional Neural Networks (CNN), as it was done in (Finch et al., 2022) for the detection of visually distinguishable ship NO_2 plumes. However, (Kurchaba et al., 2022, 2023) provide indications that CNN architecture might not be a suitable option for the detection of plumes that are poorly distinguishable on the TROPOMI data.

5. Conclusions

In this study, we investigated the sensitivity limits of the TROPOMI data-based detection system with respect to the detection of NO_2 plumes from individual seagoing ships. To the best of our knowledge, no previous research has examined this aspect, making our findings novel and significant in understanding the capabilities of the TROPOMI instrument. Our results are obtained through the analysis of four regions of interest (the Mediterranean Sea, Biscay Bay, Arabian Sea, and Bengal Bay) and can be summarized as follows:

1. We quantified the sensitivity limits of a detection system for NO_2 plumes from seagoing ships using TROPOMI data in terms of the length and speed of a ship beyond which the NO_2 plumes from individual ships cannot be distinguished anymore.
2. We also numerically showed that, as expected, the ships with higher emissions (through either greater length or speed) are more easily detected. We demonstrated such an effect by analyzing model performances with the removal from the dataset ships with the lowest emission proxy. This is agnostic to the model or studied region.
3. Then, we demonstrated that the detection of the NO_2 plumes from the ships with lower emission proxy can be improved, once more training data is added.

4. Finally, we obtained different levels of results between the studied regions. We showed that for different regions a machine learning model not only yields different levels of results but also uses different features as indicators of the presence of a plume in an image patch. A discrepancy is noticeable when comparing the Arabian Sea and Bengal Bay to the Mediterranean Sea and Biscay Bay.

To sum up, our findings suggest that, while efficient monitoring of seagoing ships from the TROPOMI satellite is possible, the quality of ship plume detectability depends on many factors. We believe our results provide guidelines for establishing the research scope for future studies on NO_2 ship plume detection as well as contribute to the successful application of satellite-based instruments for the monitoring of NO_2 emission from seagoing ships.

Author contribution

Conceptualization: S.K., A.S., J.vV., and C.J.V. Methodology: S.K., A.S., J.vV., and C.J.V. Software: S.K., A.S. Validation: S.K. Formal analysis: S.K. Investigation, S.K. Resources: S.K., J.vV., and F.J.V. Data curation: S.K, and J.vV. Writing—original draft: S.K. Writing—review and editing: C.J.V., J.vV., A.S., and F.J.V. Visualization: S.K. Supervision: C.J.V., J.vV., and F.J.V. Project administration: F.J.V. Funding acquisition: J.vV. All authors have read and agreed to the published version of the manuscript.

Declaration of competing interest

The authors declare no competing interest.

Data availability

The TROPOMI data is freely available via https://s5phub.copernicus.eu/. Starting from the product version upgrade from 1.2.2 to 1.3.0 that took place on March 27, 2019, the ECMWF operational model analyses 10 meters wind data for coinciding time is available as a support product in the TROPOMI data file. For the scope of this study, the AIS data, as well as information about the dimensions of the ships were provided to us by the ILT, which is the Dutch national designated authority for shipping inspections, is participating in this research, and has access to commercial databases of AIS data and official ship registries.

Acknowledgments

We would like to express our sincere gratitude to Charles Moussa for fruitful discussions and help with the implementation of some of the experiments presented in this study. This work is funded by the Netherlands Human Environment and Transport Inspectorate, the Dutch Ministry of Infrastructure and Water Management, and the SCIPPER project, which receives funding from the European Union's Horizon 2020 research and innovation program under grant agreement Nr.814893.

References

Agrawal, H., Malloy, Q.G., Welch, W.A., Miller, J.W., Cocker III, D.R., 2008. In-use gaseous and particulate matter emissions from a modern ocean going container vessel. Atmospheric Environment 42, 5504–5510. URL: https://doi.org/10.1016/j.atmosenv.2008.02.053, doi:10.1016/j.atmosenv.2008.02.053.

Beecken, J., Mellqvist, J., Salo, K., Ekholm, J., Jalkanen, J.P., 2014. Airborne emission measurements of so 2, no x and particles from individual ships using a sniffer technique. Atmospheric Measurement Techniques 7, 1957–1968. doi:10.5194/amt-7-1957-2014.

Berg, N., Mellqvist, J., Jalkanen, J.P., Balzani, J., 2012. Ship emissions of so 2 and no 2: Doas measurements from airborne platforms. Atmospheric Measurement Techniques 5, 1085–1098.

Cawley, G.C., Talbot, N.L., 2010. On over-fitting in model selection and subsequent selection bias in performance evaluation. The Journal of Machine Learning Research 11, 2079–2107. doi:10.5555/1756006.1859921.

Chen, T., Guestrin, C., 2016. Xgboost: A scalable tree boosting system, in: Proceedings of the 22nd acm sigkdd international conference on knowledge discovery and data mining, pp. 785–794. URL: https://doi.org/10.1145/2939672.2939785, doi:10.1145/2939672.2939785.

Corbett, J.J., Winebrake, J.J., Green, E.H., Kasibhatla, P., Eyring, V., Lauer, A., 2007. Mortality from ship emissions: a global assessment. Environmental science & technology 41, 8512–8518. URL: https://doi.org/10.1021/es071686z, doi:10.1021/es071686z.

Eskes, H., van Geffen, J., Boersma, F., Eichmann, K.U., Apituley, A., Pedergnana, M., Sneep, M., Veefkind, J.P., Loyola, D., 2022. Sentinel-5 precursor/TROPOMI Level 2 Product User Manual Nitrogendioxide. Technical Report S5P-KNMI-L2-0021-MA.

Fabian, P., 2011. Scikit-learn: Machine learning in python. Journal of machine learning research 12 , 2825doi:10.5555/1953048.2078195.

Finch, D.P., Palmer, P.I., Zhang, T., 2022. Automated detection of atmospheric no 2 plumes from satellite data: a tool to help infer anthropogenic combustion emissions. Atmospheric Measurement Techniques 15, 721–733. URL: https://doi.org/10.5194/amt-15-721-2022, doi:10.5194/amt-15-721-2022.

Friedman, J.H., Popescu, B.E., 2008. Predictive learning via rule ensembles doi:10.1214/07-AOAS148.

Georgoulias, A.K., Boersma, K.F., van Vliet, J., Zhang, X., Zanis, P., de Laat, J., et al., 2020. Detection of no2 pollution plumes from individual ships with the tropomi/s5p satellite sensor. Environmental Research Letters 15, 124037. doi:10.1088/1748-9326/abc445.

Géron, A., 2022. Hands-on machine learning with Scikit-Learn, Keras, and TensorFlow. " O'Reilly Media, Inc.".

Hastie, T., Tibshirani, R., Friedman, J.H., Friedman, J.H., 2009. The elements of statistical learning: data mining, inference, and prediction. volume 2. Springer. doi:10.1007/978-0-387-21606-5.

IMO, 1997. Amendments to the annex of the protocol of 1978 relating to the international convention for the prevention of pollution from ships. URL:

https://wwwcdn.imo.org/localresources/en/KnowledgeCentre/IndexofIMOResolutions/MEPCDocuments/MEPC.75(40).pdf.

IMO, 2020. Marpol annex vi - regulation 13. URL: https://www.imo.org/en/OurWork/Environment/Pages/Nitrogen-oxides-(NOx)-%E2%80%93-Regulation-13.aspx.

Kurchaba, S., Sokolovsky, A., Van Vliet, J., Verbeek, F.J., Veenman, C.J., 2024. Sensitivity analysis for the detection no2 plumes from seagoing ships using tropomi data. reproducibility package. URL: https://codeocean.com/capsule/0324035/tree/v1, doi:10.24433/CO.8459888.V1.

Kurchaba, S., van Vliet, J., Meulman, J.J., Verbeek, F.J., Veenman, C.J., 2021. Improving evaluation of no2 emission from ships using spatial association on tropomi satellite data, in: 29th International Conference on Advances in Geographic Information Systems, pp. 454–457. URL: https://doi.org/10.1145/3474717.3484213, doi:10.1145/3474717.3484213.

Kurchaba, S., van Vliet, J., Verbeek, F.J., Meulman, J.J., Veenman, C.J., 2022. Supervised segmentation of no2 plumes from individual ships using tropomi satellite data. Remote Sensing 14. URL: https://www.mdpi.com/2072-4292/14/22/5809, doi:10.3390/rs14225809.

Kurchaba, S., van Vliet, J., Verbeek, F.J., Veenman, C.J., 2023. Anomalous no2 emitting ship detection with tropomi satellite data and machine learning. Remote Sensing of Environment 297, 113761.

Lack, D.A., Corbett, J.J., Onasch, T., Lerner, B., Massoli, P., Quinn, P.K., Bates, T.S., Covert, D.S., Coffman, D., Sierau, B., et al., 2009. Particulate emissions from commercial shipping: Chemical, physical, and optical properties. Journal of Geophysical Research: Atmospheres 114.

Landgraf, J., Rusli, S., Cooney, R., Veefkind, P., Vemmix, T., de Groot, Z., Bell, A., Day, J., Leemhuis, A., Sierk, B., 2020. The tango mission: A satellite tandem to measure major sources of anthropogenic greenhouse gas emissions, in: EGU General Assembly Conference Abstracts, p. 19643.

Lundberg, S.M., Lee, S.I., 2017. A unified approach to interpreting model predictions. Advances in neural information processing systems 30.

McLaren, R., Wojtal, P., Halla, J.D., Mihele, C., Brook, J.R., 2012. A survey of no2: So2 emission ratios measured in marine vessel plumes in the strait of georgia. Atmospheric environment 46, 655–658. URL: https://doi.org/10.1016/j.atmosenv.2011.10.044, doi:10.1016/j.atmosenv.2011.10.044.

Mou, J.M., Van der Tak, C., Ligteringen, H., 2010. Study on collision avoidance in busy waterways by using ais data. Ocean Engineering 37, 483–490. URL: https://doi.org/10.1016/j.oceaneng.2010.01.012, doi:10.1016/j.oceaneng.2010.01.012.

Pirjola, L., Pajunoja, A., Walden, J., Jalkanen, J.P., Rönkkö, T., Kousa, A., Koskentalo, T., 2014. Mobile measurements of ship emissions in two harbour areas in finland. Atmospheric Measurement Techniques 7, 149–161.

Schreier, S., Peters, E., Richter, A., Lampel, J., Wittrock, F., Burrows, J.,

2015. Ship-based max-doas measurements of tropospheric no2 and so2 in the south china and sulu sea. Atmospheric Environment 102, 331–343.

Sneep, M., 2021. Sentinel 5 precursor/TROPOMI KNMI and SRON level 2 Input Output Data Definition. Technical Report S5P-KNMI-L2-0009-SD.

Stone, M., 1974. Cross-validation and multinomial prediction. Biometrika 61, 509–515. URL: https://doi.org/10.1093/biomet/61.3.509, doi:10.1093/biomet/61.3.509.

Van Roy, W., Scheldeman, K., 2016. Results marpol annex vi monitoring report: Belgian sniffer campaign 2016 .

Veefkind, J., Aben, I., McMullan, K., Förster, H., De Vries, J., Otter, G., Claas, J., Eskes, H., De Haan, J., Kleipool, Q., et al., 2012. Tropomi on the esa sentinel-5 precursor: A gmes mission for global observations of the atmospheric composition for climate, air quality and ozone layer applications. Remote sensing of environment 120, 70–83. URL: https://doi.org/10.1016/j.rse.2011.09.027, doi:10.1016/j.rse.2011.09.027.

Vinken, G.C., Boersma, K.F., Jacob, D.J., Meijer, E.W., 2011. Accounting for non-linear chemistry of ship plumes in the geos-chem global chemistry transport model. Atmospheric Chemistry and Physics 11, 11707–11722. doi:10.5194/acp-11-11707-2011.

List of Figures

Region	Ship image	No ship image
Mediterranean	16%	18%
Biscay Bay	48%	52%
Arabian Sea	49%	52%
Bengal Bay	54%	54%

Table A.6: Percentage of data from the original dataset lost when qa .75 filtered applied.

Appendices

Appendix A Assessment of data loss as a result stricter filtering

In Table A.6, we show the percentage of the data that would be lost if the filtering criterion qa$\geq$0.75 was applied.

Appendix B Data distributions

In Figure B.15, we provide the distribution of the features that are used in the dataset of this study.

Appendix C Hyperparameters' search space

In this Section of the Appendix, we provide the hyperparameters' search space used for the optimization of the performance of the model.

- **Logistic**(solver='saga', l1_ratio=0.5, random_state=0)

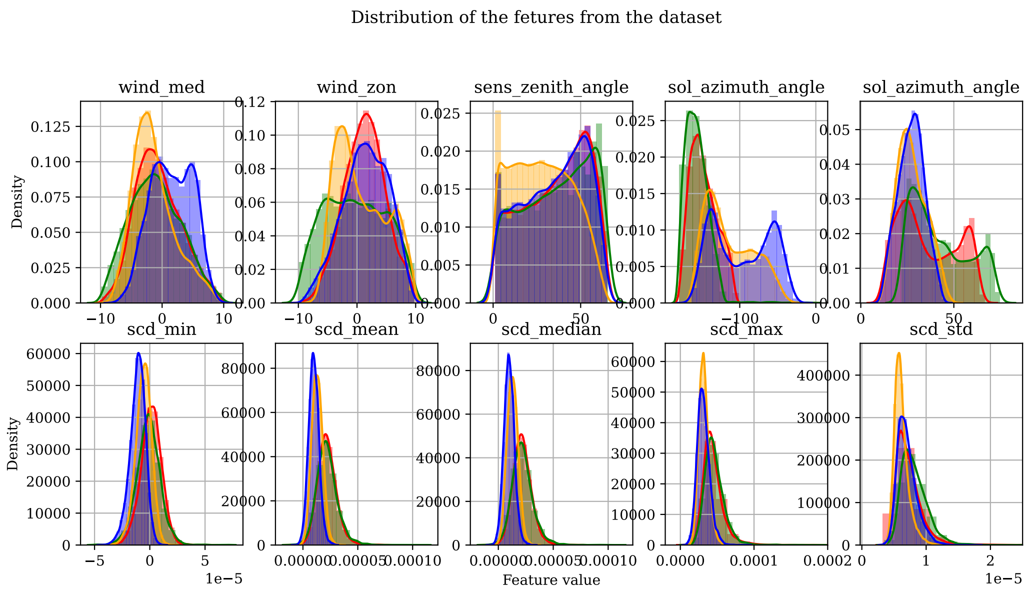

Figure B.15: Histograms of the variables from the dataset.

- penalty: ('l1', 'l2', 'elasticnet', 'none')
- C: (0.0001, 0.001, 0.1, 1)
- max_iter: (100, 120, 150)

- **SVM**(kernel='rbf', gamma = 'scale', random_state=0, probability=True)
    - C: (2.0e-2, 0.5e-1, 1.0e-1, 1.5e-1, 2.0e-1, 2.5e-1, 2.0)
- **Random Forest**(random_state=0)
    - n_estimators: [10, 20, 50, 100, 150, 500]
    - min_samples_leaf: [2; 36]
    - min_samples_split: [2, 30]
    - max_features: ('sqrt', 0.4, 0.5)

- criterion: ('gini', 'entropy')
- bootstrap: (True, False)

- **XGB**(random_state=0)
  - n_estimators: [10, 20, 50, 100, 150, 500]
  - gamma: [0.05; 0.5]
  - max_depth: (2, 3, 5, 6)
  - min_child_weight: (2, 4, 6, 8, 10, 12)
  - subsample: [0.6; 1.0]
  - learning_rate: [1e-3, 1e-2, 1e-1, 0.5, 1.0]
  - reg_alpha: (0, 1.0e-5, 5.0e-4, 1.0e-3, 1.0e-2, 0.1, 1)

Appendix D Optimized set of hyperparameters

Then, we provide the set of hyperparameters that was selected as optimal for each model at each iteration of cross-validation for each studied region. The results of the performance of the corresponding models are presented in Table 4.

Mediterranean Sea

- **Logistic**(solver='saga', l1_ratio=0.5, random_state=0)
  - **penalty:** CV1: 'l2'; CV2: 'l2'; CV3: 'l2'; CV4: 'l2'; CV5: 'elasticnet';
  - **C:** CV1: 0.001; CV2: 1; CV3: 0.0001; CV4: 0.001; CV5: 0.1;

- **max_iter:** CV1: 100; CV2: 100; CV3: 100; CV4: 100; CV5: 150;

- **SVM**(kernel='rbf', gamma = 'scale', random_state=0, probability=True)
  - **C:** CV1: 2; CV2: 2; CV3: 2; CV4: 2; CV5: 2;

- **Random Forest**(random_state=0)
  - **n_estimators:** CV1: 500; CV2: 500; CV3: 500; CV4: 500; CV5: 500;
  - **min_samples_split:** CV1: 12; CV2: 12; CV3: 12; CV4: 12; CV5: 12;
  - **min_samples_leaf:** CV1: 1; CV2: 1; CV3: 1; CV4: 1; CV5: 1;
  - **max_features:** CV1: 'sqrt'; CV2: 'sqrt'; CV3: 'sqrt'; CV4: 'sqrt'; CV5: 'sqrt';
  - **criterion:** CV1: 'gini'; CV2: 'gini'; CV3: 'gini'; CV4: 'gini'; CV5: 'gini';
  - **bootstrap:** CV1: True; CV2: True; CV3: True; CV4: True; CV5: True;

- **XGB**(random_state=0)
  - **n_estimators:** CV1: 150; CV2: 500; CV3: 150; CV4: 500; CV5: 150;
  - **gamma:** CV1: 0.05; CV2: 0.3; CV3: 0.05; CV4: 0.05; CV5: 0.05;
  - **max_depth:** CV1: 6; CV2: 6; CV3: 6; CV4: 6; CV5: 6;
  - **min_child_weight:** CV1: 8; CV2: 8; CV3: 8; CV4: 10; CV5: 8;

  - **subsample:** CV1: 0.89; CV2: 0.6; CV3: 0.89; CV4: 0.7; CV5: 0.89;
  - **learning_rate:** CV1: 0.01; CV2: 0.01; CV3: 0.01; CV4: 0.01; CV5: 0.01;
  - **reg_alpha:** CV1: 1e-02; CV2: 1e-05; CV3: 1e-02; CV4: 5e-04; CV5: 1e-02;

Biscay Bay

- **Logistic**(solver='saga', l1_ratio=0.5, random_state=0)
  - **penalty:** CV1: 'elasticnet'; CV2: 'none'; CV3: 'none'; CV4: 'none'; CV5: 'l1';
  - **C:** CV1: 1; CV2: 0.0001; CV3: 0.0001; CV4: 0.0001; CV5: 1;
  - **max_iter:** CV1: 100; CV2: 100; CV3: 100; CV4: 100; CV5: 100;
- **SVM**(kernel='rbf', gamma = 'scale', random_state=0, probability=True)
  - **C:** CV1: 2; CV2: 2; CV3: 2; CV4: 2; CV5: 2;
- **Random Forest**(random_state=0)
  - **n_estimators:** CV1: 100; CV2: 150; CV3: 500; CV4: 500; CV5: 500;
  - **min_samples_split:** CV1: 2; CV2: 27; CV3: 22; CV4: 22; CV5: 22;
  - **min_samples_leaf:** CV1: 7; CV2: 10; CV3: 10; CV4: 10; CV5: 10;

  - **max_features:** CV1: None; CV2: None; CV3: None; CV4: None; CV5: None;
  - **criterion:** CV1: 'entropy'; CV2: 'entropy'; CV3: 'entropy'; CV4: 'entropy'; CV5: 'entropy';
  - **bootstrap:** CV1: True; CV2: True; CV3: True; CV4: True; CV5: True;

- **XGB**(random_state=0)
  - **n_estimators:** CV1: 150; CV2: 150; CV3: 100; CV4: 150; CV5: 100;
  - **gamma:** CV1: 0.05; CV2: 0.05; CV3: 0.4; CV4: 0.05; CV5: 0.4;
  - **max_depth:** CV1: 6; CV2: 6; CV3: 6; CV4: 6; CV5: 6;
  - **min_child_weight:** CV1: 8; CV2: 8; CV3: 2; CV4: 8; CV5: 2;
  - **subsample:** CV1: 0.89; CV2: 0.89; CV3: 0.89; CV4: 0.89; CV5: 0.89;
  - **learning_rate:** CV1: 0.1; CV2: 0.1; CV3: 0.1; CV4: 0.1; CV5: 0.1;
  - **reg_alpha:** CV1: 1e-02; CV2: 1e-02; CV3: 1e-01; CV4: 1e-02; CV5: 1e-01;

Arabian Sea

- **Logistic**(solver='saga', l1_ratio=0.5, random_state=0)
  - **penalty:** CV1: 'l1'; CV2: 'elasticnet'; CV3: 'l1'; CV4: 'l1'; CV5: 'l1';

  - **C:** CV1: 0.001; CV2: 0.001; CV3: 0.001; CV4: 0.001; CV5: 0.001;
  - **max_iter:** CV1: 100; CV2: 150; CV3: 120; CV4: 100; CV5: 120;
- **SVM**(kernel='rbf', gamma = 'scale', random_state=0, probability=True)
  - **C:** CV1: 0.15; CV2: 0.05; CV3: 0.25; CV4: 0.25; CV5: 0.2;
- **Random Forest**(random_state=0)
  - **n_estimators:** CV1: 500; CV2: 500; CV3: 500; CV4: 500; CV5: 500;
  - **min_samples_split:** CV1: 22; CV2: 22; CV3: 7; CV4: 7; CV5: 7;
  - **min_samples_leaf:** CV1: 10; CV2: 10; CV3: 7; CV4: 7; CV5: 7;
  - **max_features:** CV1: None; CV2: None; CV3: 'sqrt'; CV4: 'sqrt'; CV5: 'sqrt';
  - **criterion:** CV1: 'entropy'; CV2: 'entropy'; CV3: 'entropy'; CV4: 'entropy'; CV5: 'entropy';
  - **bootstrap:** CV1: True; CV2: True; CV3: True; CV4: True; CV5: True;
- **XGB**(random_state=0)
  - **n_estimators:** CV1: 500; CV2: 500; CV3: 500; CV4: 500; CV5: 500;
  - **gamma:** CV1: 0.3; CV2: 0.3; CV3: 0.3; CV4: 0.3; CV5: 0.3;

  - **max_depth:** CV1: 6; CV2: 6; CV3: 6; CV4: 6; CV5: 6;
  - **min_child_weight:** CV1: 8; CV2: 10; CV3: 8; CV4: 10; CV5: 10;
  - **subsample:** CV1: 0.6; CV2: 0.6; CV3: 0.6; CV4: 0.6; CV5: 0.6;
  - **learning_rate:** CV1: 0.01; CV2: 0.01; CV3: 0.01; CV4: 0.01; CV5: 0.01;
  - **reg_alpha:** CV1: 1e-05; CV2: 1e-05; CV3: 1e-05; CV4: 1e-05; CV5: 1e-05;

Bengal Bay

- **Logistic**(solver='saga', l1_ratio=0.5, random_state=0)
  - **penalty:** CV1: 'l2'; CV2: 'l2'; CV3: 'elasticnet'; CV4: 'l1'; CV5: 'none';
  - **C:** CV1: 0.1; CV2: 1; CV3: 0.001; CV4: 1; CV5: 0.0001;
  - **max_iter:** CV1: 150; CV2: 150; CV3: 100; CV4: 150; CV5: 150;
- **SVM**(kernel='rbf', gamma = 'scale', random_state=0, probability=True)
  - **C:** CV1: 0.15; CV2: 0.25; CV3: 0.05; CV4: 0.25; CV5: 0.1;
- **Random Forest**(random_state=0)
  - **n_estimators:** CV1: 500; CV2: 500; CV3: 150; CV4: 500; CV5: 500;
  - **min_samples_split:** CV1: 2; CV2: 2; CV3: 12; CV4: 2; CV5: 2;

  - **min_samples_leaf:** CV1: 16; CV2: 16; CV3: 19; CV4: 16; CV5: 16;
  - **max_features:** CV1: 'sqrt'; CV2: 'sqrt'; CV3: None; CV4: 'sqrt'; CV5: 'sqrt';
  - **criterion:** CV1: 'entropy'; CV2: 'entropy'; CV3: 'entropy'; CV4: 'entropy'; CV5: 'entropy';
  - **bootstrap:** CV1: True; CV2: True; CV3: True; CV4: True; CV5: True;

- **XGB**(random_state=0)
  - **n_estimators:** CV1: 100; CV2: 500; CV3: 500; CV4: 500; CV5: 50;
  - **gamma:** CV1: 0.25; CV2: 0.3; CV3: 0.3; CV4: 0.3; CV5: 0.15;
  - **max_depth:** CV1: 2; CV2: 6; CV3: 6; CV4: 6; CV5: 3;
  - **min_child_weight:** CV1: 6; CV2: 8; CV3: 8; CV4: 8; CV5: 6;
  - **subsample:** CV1: 0.7; CV2: 0.6; CV3: 0.6; CV4: 0.6; CV5: 0.89;
  - **learning_rate:** CV1: 0.1; CV2: 0.01; CV3: 0.01; CV4: 0.01; CV5: 0.1;
  - **reg_alpha:** CV1: 1e-02; CV2: 1e-05; CV3: 1e-05; CV4: 1e-05; CV5: 1;